Two-state on-off intermittency caused by unstable dimension variability in periodically forced drift waves

P. P. Galuzio, S. R. Lopes, and R. L. Viana*

Departamento de Física, Universidade Federal do Paraná, Caixa Postal 19044, 81531-990 Curitiba, Paraná, Brazil

(Received 19 July 2011; revised manuscript received 21 September 2011; published 14 November 2011)

Certain high-dimensional dynamical systems present two or more attractors characterized by different energy branches. For some parameter values the dynamics oscillates between these two branches in a seemingly random fashion, a phenomenon called two-state on-off intermittency. In this work we show that the dynamical mechanism underlying this intermittency involves the severe breakdown of hyperbolicity of the attractors through a mechanism known as unstable dimension variability. We characterize the parametric evolution of this variability using statistical properties of the finite-time Lyapunov exponents. As a model system that exhibits this behavior we consider periodically forced and damped drift waves. In this spatiotemporal example there is a low-dimensional chaotic attractor that is created by an interior crisis, already presenting unstable dimension variability.

DOI: 10.1103/PhysRevE.84.056211 PACS number(s): 05.45.Jn, 52.35.Kt

I. INTRODUCTION

While the chaotic dynamics of low-dimensional systems is by now a well-established subject with an impressive body of theoretical, numerical, and experimental results, the spatiotemporal dynamics of high-dimensional systems still has unsolved problems and big challenges [1]. Probably the hardest problem of all is the understanding of the dynamical mechanisms leading to turbulence, or spatiotemporal chaos, in fluids, plasmas, and other spatially extended systems [2].

One of the promising approaches to this problem is a description of the onset of turbulence as when the system energy, originally concentrated in the temporal degree of freedom and a few spatial modes (a traveling wave), starts to be distributed among the remaining spatial degrees of freedom. Such a description is particularly suited for being described by Fourier mode expansions, where each mode is a degree of freedom. In order to accomplish this transition the temporal dynamics must present a chaotic attractor acting as a stochastic pump, by feeding energy to the spatial modes to be excited so as to result in irregular spatial behavior [3,4].

A geometrical view of this phenomenon is possible in the Fourier phase space (i.e., the space whose variables are the Fourier modes), if we regard the temporal dynamics as occurring in a low-dimensional attractor embedded in the phase space. There are just a few spatial degrees of freedom excited therein, and we can think of the system as displaying a spatially ordered pattern. In the following, all the other spatial modes that are not excited will be called transversal with respect to the chaotic attractor. The onset of spatiotemporal chaos occurs when the temporally chaotic attractor loses transversal stability such that the trajectories are allowed to explore more spatial degrees of freedom, imparting energy to the corresponding spatial modes [5].

A further development of the previous analysis consists on considering two different states with the above-mentioned properties instead of only one. This case is physically interesting because many spatiotemporal systems display two (or more) solution branches, each of them with the characteristics of a chaotic attractor [6]. One outstanding example is the damped and periodically forced nonlinear drift-wave equation, which occurs, e.g., in magnetized plasmas with temperature or density gradients [7] and in the atmospheric vortex flows (with the name Rossby waves) with Coriolis force gradients [8].

The damped and periodically forced drift-wave equation has been found to present two stationary solutions (depending on the driving amplitude) with different wave energies that lie on different branches of the Fourier phase space [9], which we identify with the two chaotic attractors. We have recently found that the onset of turbulence in this system follows the breakdown of transversal stability of these attractors [10]. Moreover, it may well happen that both attractors are simultaneously unstable in the transversal directions to them. In this case the trajectories wander through the available phase-space volume approaching the vicinity of the both attractors in an erratic way.

This latter situation leads to the so-called two-state on-off intermittency, for there is an alternating behavior between two different stationary states [11,12]. In spatially extended systems the dynamics at either state lies near an attractor embedded in the phase space. Starting from an initial condition very close to either attractor, the ensuing trajectory goes to the vicinity of another state, the transient behavior in between these states being governed by a chaotic saddle [13]. Due to the chaotic behavior governing the dynamics in each state, these alternations occur for different and irregularly spaced time intervals.

In this paper we pursue a complementary, yet novel, description of the occurrence and evolution of two-state on-off intermittency, which is its relation with a severe breakdown of hyperbolicity in the chaotic attractors involved in the process. This breakdown occurs whenever there are periodic orbits embedded in either attractor with different numbers of unstable directions, a phenomenon called *unstable dimension variability* (UDV) [14].

The absence of shadowing trajectories long enough to warrant numerical computations using chaotic pseudotrajectories is one of the consequences of UDV in a chaotic dynamical system [15]. One may argue that this does not seem to be

*viana@fisica.ufpr.br

an essential difficulty, since the interesting quantities to be computed from nonshadowable chaotic trajectories are of statistical nature, like averages and variances [16]. However, if there is UDV, even statistical quantities may be plagued with an uncontrollable amplification of the noise inherent to computer-generated trajectories [17].

The connection between UDV and on-off intermittency has been pursued by us in earlier papers [18]. Since the onset of UDV involves the loss of transversal stability of periodic orbits embedded in chaotic attractors, if there is more than one attractor it may happen that the trajectory is repeatedly repelled from both attractors, which is two-state on-off intermittency. Actually we have this scenario only after both attractors lose transversal stability as a whole (the critical condition being called a blowout bifurcation). The main result of the present paper is that two-state on-off intermittency implies the existence of UDV in both attractors.

In order to characterize the parametric evolution of UDV we used the well-known fact that, when there is UDV, the finite-time Lyapunov exponent nearest to zero fluctuates about zero. This is ultimately due to visits of the trajectory to regions of the attractor with a varying number of stable and unstable directions [19].

This paper is organized as follows: In Sec. II we describe the periodically forced and damped drift-wave equations, which is a theoretical model for which the existence of two-state on-off intermittency has been shown to occur for certain parameter ranges. Section III deals with the connection between the intermittent behavior and the loss of transversal stability of the coexisting solutions of the forced drift-wave equation. Section IV considers the Lyapunov spectrum of the system. Section V brings about numerical results on the onset and the parametric evolution of UDV in a simple example and the forced and damped drift-wave equation, using the statistical properties of the finite-time Lyapunov exponents. Our conclusions are left to the final section.

II. PERIODICALLY FORCED DRIFT WAVES

Drift waves appear in two distinct but closely related physical settings. In magnetically confined fusion plasmas with temperatures or density gradients, low-frequency drift waves are found to be either unstable or exponentially damped, depending on the wave vector and the plasma properties [7,20]. In geophysical fluid flows the corresponding Rossby waves appear in geostrophic rotating flows, the Coriolis force playing the same role as the Lorentz force in the plasma drift waves [8].

Both problems are quasi-two-dimensional, for the main velocity components lie in a plane. For plasma drift waves this plane is perpendicular to the magnetic field, and the electric potential $\phi(x,t)$ (in the one-dimensional case) satisfies the drift-wave equation

$$\phi_t + a\phi_{txx} + c\phi_x + f\phi\phi_x = 0. \tag{1}$$

For magnetically confined fusion plasmas $\phi(x,t)$ is the nondimensional electric potential of a drift wave propagating along the poloidal direction of a toroidal plasma. The parameters a, c, and f are related to the ion gyrofrequency, the density gradient and the ion acoustic speed of the plasma [21]. In Rossby waves ϕ would stand for the variable part of the fluid depth, and the parameters above are related to the gravity wave speed, the Coriolis parameter, and the Rossby radius [8].

The unforced drift wave has three constants of motion:

$$E_1 = \frac{1}{2\pi}\int_0^{2\pi} \phi(x,t)\,dx, \tag{2}$$

$$E_2 = \frac{1}{2\pi}\int_0^{2\pi} \left[\phi^2(x,t) - a\phi_x^2(x,t)\right]dx, \tag{3}$$

$$E_3 = \frac{1}{2\pi}\int_0^{2\pi} \left[c\phi^2(x,t) + \frac{1}{3}f\phi^3(x,t)\right]dx, \tag{4}$$

corresponding, respectively, to "mass," momentum, and Hamiltonian. In plasma physics we usually refer to E_2 as the "wave energy" and denote it simply by E. In spite of the existence of these constants, however, the unforced drift-wave equation is a nonintegrable system, which allows the existence of complex dynamics.

In plasma experiments there has been found that the electric potential fluctuation spectrum is broadly distributed around the drift-wave frequency, what suggests the existence of strong mode interactions [22]. We can model such interactions with other modes by adding to the drift-wave equation a time-periodic driving with amplitude ϵ, wave number K, and frequency Ω. Moreover, to have bounded solutions of the forced equation it is necessary also to introduce a phenomenological linear damping term with coefficient γ [9]. The resulting equation is

$$\phi_t + a\phi_{txx} + c\phi_x + f\phi\phi_x + \gamma\phi = -\epsilon\sin(Kx - \Omega t). \tag{5}$$

Since the x coordinate is a bounded variable, we suppose a Fourier mode expansion

$$\phi(x,t) = \sum_{n=-(N/2)+1}^{N/2} \phi_n(t)e^{i\kappa_n x}, \tag{6}$$

where $\phi_n(t)$ are the corresponding mode amplitudes, and the corresponding wave number is related to the box length $L = 2\pi$ (we adopt periodic boundary conditions) by

$$\kappa_n \equiv \frac{2\pi n}{L}. \tag{7}$$

In the N-dimensional Fourier phase space the variables are the mode amplitudes ϕ_n, whose time evolution is governed by a vector field obtained by substituting (6) into (5). The mode amplitude ϕ_0, for which $\kappa_0 = 0$, is purely temporal, whereas ϕ_α ($\alpha = 1,\ldots,N$), for which $\kappa_\alpha = \alpha$, are spatial modes.

We used $N = 128$ modes for numerically solving Eq. (5), and the following parameters [9]: $a = -0.28711$, $c = 1.0$, $f = -6.0$, $\gamma = 0.1$, $K = 1.0$, and $\Omega = 0.65$, such that the forcing amplitude ϵ will be our control parameter. The initial conditions for the system of N coupled mode equations are

$$\phi_1(0) = \sigma_1 R(0,1), \quad \phi_2(0) = \sigma_2 R(0,1), \tag{8}$$

$$\phi_n(0) = \sigma_3, \quad (n = 0, 34\ldots), \tag{9}$$

where $\sigma_1 = 0.1$, $\sigma_2 = 0.01$, $\sigma_3 = 10^{-5}$, and $R(0,1)$ is a pseudorandom number chosen within the interval $[0,1]$ with uniform probability.

Since we are working in the Fourier phase space, a useful quantity to characterize the dissipative system is the wave

momentum (3). According to the customary usage we shall call it "wave energy" $E(t)$. Even though, for certain parameter values, the wave dynamics may be chaotic, nevertheless the energy difference is always bounded [21,23,24]. In fact, we have found two energy states, each of them being characterized by a chaotic attractor, which we may regard as belonging to a manifold embedded in the Fourier phase space.

One of such manifolds is low dimensional (in the Fourier phase space) since its dynamics is chaotic in time and just a few spatial modes are excited, corresponding to stationary state, which is a steady wave propagating in space whose amplitude is evolving chaotically. On the other hand, the other manifold presents a spatiotemporal chaotic state, which we may identify as a weak form of turbulence, which requires the excitation of a large number of spatial modes. Hence the manifold corresponding to this second state has a larger dimension than the first state, although both are low-dimensional compared with the simulated Fourier phase-space dimension.

III. LOSS OF TRANSVERSAL STABILITY

The time evolution of the wave energy $E(t)$ versus the forcing amplitude ϵ is depicted in Fig. 1 and illustrates this coexistence of distinct energy branches. For $\epsilon = 0.192$ [Fig. 1(a)] the system is in one of these branches (the upper limit of which is indicated by a red line), undergoing periodic motion (as confirmed by Lyapunov exponents, as we shall see later).

We geometrically interpret this result as a consequence of the dynamics being restricted to a lower energy state characterized by energy fluctuations about $E_0 \approx 0.03$ with amplitude not larger than $E_{\text{thres}} = 0.07$ (this threshold has been indicated as a red line in Fig. 1). In Fig. 2 we indicate this average as a black thick line (dashed if the manifold is transversely unstable) and the corresponding fluctuations by a gray strip, bounded from above by a dotted line that stands for the threshold of the lower energy state.

A slight increase in the value of ϵ leads to bursts of chaotic behavior followed by a slow return to the lower-energy branch, where the evolution is now temporally chaotic [Fig. 1(b)]. This change is due to a transition occurring at $\epsilon_t = 0.192\,50 \pm 0.000\,01$, whereby some unstable periodic orbits embedded in the attractor lying on the lower-energy manifold lose transversal stability (in terms of the transversal directions of the Fourier phase space related to the spatial degrees of freedom). The error bars refer to the finite time of the numerical simulations performed (for the sake of simplicity we shall omit the error bars whenever possible).

Let us consider this transition in some more detail. The loss of transversal stability of a chaotic attractor, as a given tunable parameter is varied through a critical value, has been described by three mechanisms. The first of them, known as *bubbling transition* or *riddling bifurcation*, describes the loss of transversal stability when a low-period periodic orbit embedded in the chaotic set loses transversal stability [25]. The second mechanism, closely related to the first one, involves an unstable periodic orbit whose period goes to infinity as we approach the point where there is loss of transversal stability [26]. It is important to emphasize that these two mechanisms require the existence of invariant manifolds where the chaotic attractors lie, a requirement that cannot be demonstrated in the drift-wave equations considered in this work.

On the other hand, the third mechanism for the loss of transversal stability, described by some of the authors in a previous work [27], does not require the existence of an invariant subspace with a chaotic attractor in the phase space. The loss of transversal stability is triggered by an interior crisis, or a collision between a chaotic attractor and an unstable periodic orbit [28]. This *crisis-induced scenario* has been exemplified by the kicked double rotor map [27]. The chaotic attractor is already born with orbits possessing different numbers of transversely unstable directions. In other words, as soon as the attractor is created, some periodic orbits

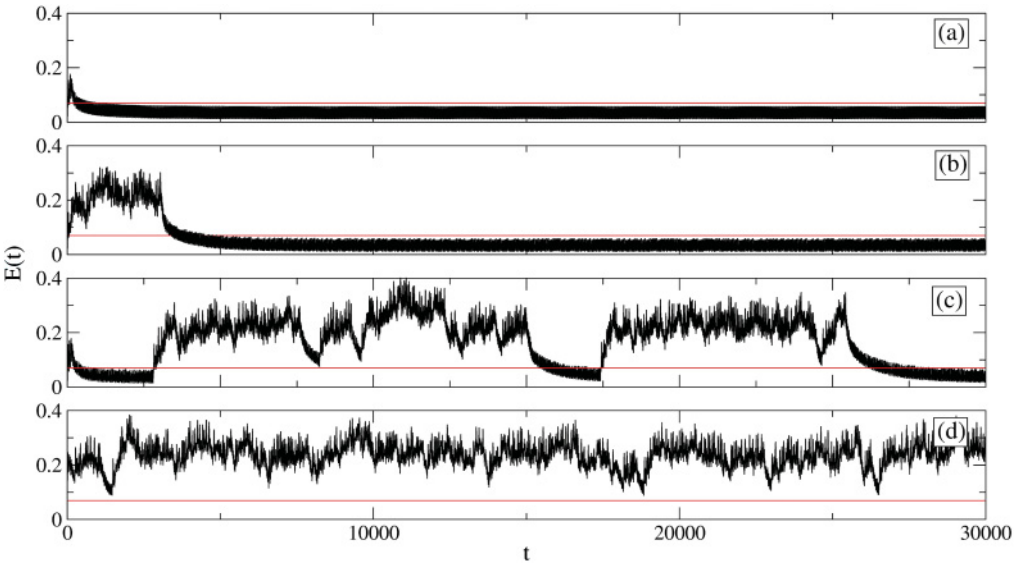

FIG. 1. (Color online) Time evolution of the energy difference for $\epsilon =$ (a) $0.1920 < \epsilon_t$; (b) $\epsilon_t < 0.1950 < \epsilon_\ell$; (c) $\epsilon_\ell < 0.2003 < \epsilon_h$; (d) $0.2030 > \epsilon_h$. The red line marks the limit of bounded variation for the fluctuations in the lower-energy branch.

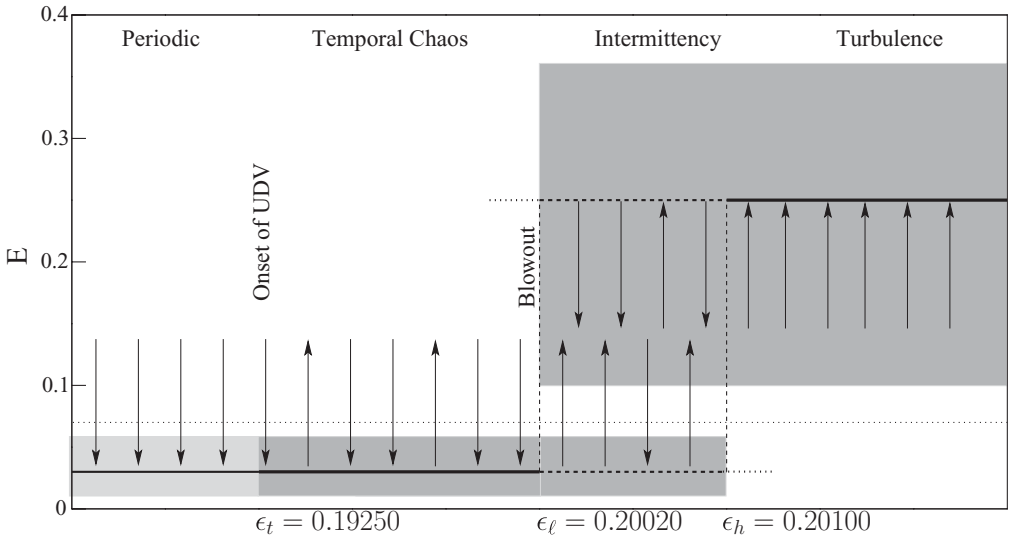

FIG. 2. Schematic figure showing the two energy states and their corresponding transversal stability. The shaded regions represent the intervals of bounded variation of energy fluctuations about their average values (shown as solid and dashed lines for transversely stable and unstable cases, respectively).

embedded in it have different unstable dimensions. We shall quantitatively characterize this property in the next section.

The other reason, illustrated by the bifurcation diagram displayed in Fig. 3, is that, at the point where some periodic orbit embedded in the lower energy manifold loses transversal stability—namely, at $\epsilon_t = 0.192\,50$—there is a sudden appearance of a chaotic attractor out of a low-period stable orbit that exists for $\epsilon \lesssim \epsilon_t$. Viewed from the opposite direction, the chaotic attractor that exists for $\epsilon \gtrsim \epsilon_t$ suddenly disappears due to an interior crisis: its collision with a low-period unstable orbit, yielding only a low-period stable orbit for $\epsilon \lesssim \epsilon_t$. We remark that most of the periodic orbits embedded in the lower energy manifold remain transversely stable as long as $\epsilon_t < \epsilon < \epsilon_\ell$.

Now we return to the parametric evolution of the manifolds just after the point $\epsilon = \epsilon_t$, where some low-period unstable orbit embedded in lower energy state loses transversal stability due to an interior crisis. Because "most" (in the measure-theoretical sense) of the unstable periodic orbits in the lower energy manifold remain transversely stable, however, these off-manifold chaotic bursts eventually decay back to the manifold. The ensuing behavior is practically indistinguishable to that before the transition has occurred, except for its transient nature. In terms of the scheme depicted in Fig. 2 we identify the upper limit of the lower energy state (in which some, but not all, periodic orbits have became transversely unstable) as a dotted line.

A further increase of ϵ will generate bursts of activity during which the system makes frequent excursions to the upper energy branch and also visits to the vicinity of the lower energy manifold [Fig. 1(c)]. These excursions bring the system to a higher energy state characterized by energy

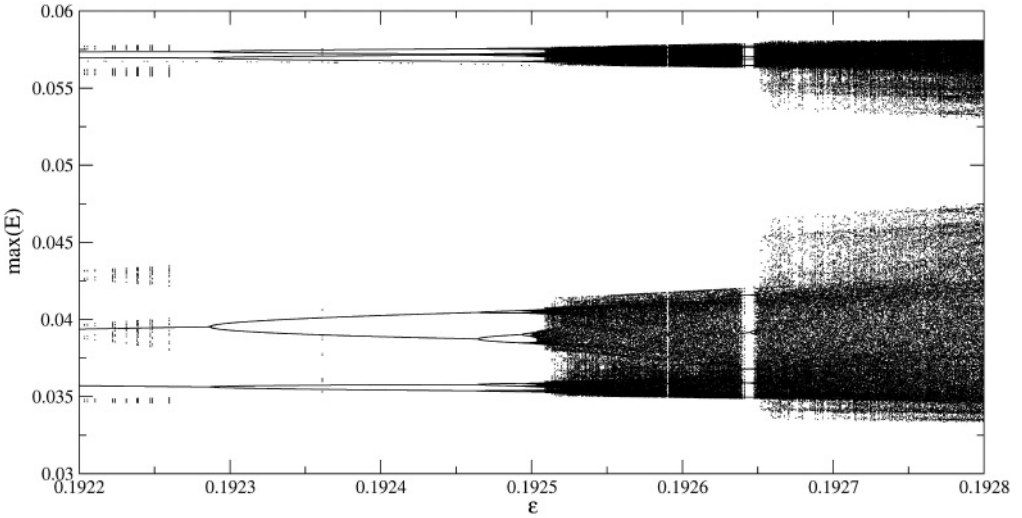

FIG. 3. Bifurcation diagram for the maximum energy value *versus* the control parameter ϵ (the strength of the forcing term). The remaining parameters are the same as used in Fig. 1.

fluctuations about $E_1 \approx 0.25$ with larger amplitudes belonging to the interval [0.1,0.35]. In Fig. 2 we indicate this average as a thick line (dashed if the manifold is transversely unstable) and the corresponding fluctuations by a gray strip, bounded from below by the same dotted line used for the threshold of lower energy state. It is of paramount importance that the fluctuation intervals do not overlap, so as to characterize the existence of two distinct energy branches.

The qualitatively different behavior shown in Fig. 1(c) suggests that another transition has occurred. Since the excursions off the lower energy state do not die off the manifold itself has became transversely unstable. In other words, the periodic orbits embedded in the lower energy manifold become transversely unstable at $\epsilon_\ell = 0.200\,20 \pm 0.000\,25$. This is known as a *blowout bifurcation* [29]. On the other hand, since the higher energy manifold is also transversely unstable by itself, the bursting excursions to and from both manifolds are not a transient effect. To this regime we call *two-state on-off intermittency*.

The intermittent regime existing for $\epsilon \gtrsim \epsilon_\ell$ disappears, however, for higher values of ϵ, namely, after another transition occurs at $\epsilon_h = 0.201\,00 \pm 0.000\,50$. After this transition the higher energy manifold becomes transversely stable, since the energy fluctuations about the higher energy average E_1 *do not cross the energy threshold* E_{thres}, as illustrated by Fig. 1(d). Hence the chaotic attractor embedded in the higher energy manifold is expected to have mostly (and perhaps all) periodic orbits that are transversely stable.

IV. LYAPUNOV SPECTRUM

The Lyapunov spectrum analysis in Fourier space is based on the idea that each Fourier mode in the discrete transform (6) can be considered a degree of freedom, and the corresponding Lyapunov exponent is computed from the algorithm proposed by Benettin *et al*. [30], with the dynamics given by the set of N ordinary differential equations for the wave amplitudes $\phi_n(t)$, with $n = 0, 1, 2, \ldots, N$.

The interpretation of the Lyapunov exponents in terms of the Fourier modes is usually difficult since the vector associated with each Lyapunov exponent is a mixture of many Fourier modes, in general. However, for small values of ϵ ($\epsilon < \epsilon_\ell$, to be more precise), the asymptotic dynamics is restricted to the lower energy state, hence the Lyapunov exponent related to $i = 0$ corresponds to the temporal dynamics, whereas the $i \geqslant 1$ case stands for spatial degrees of freedom and can be used to detect spatial mode excitation [31].

Accordingly in Fig. 4 we plot the asymptotic value of the 30 first Lyapunov exponents out of $N = 128$ modes corresponding to the wave amplitudes in Eq. (6). In the latter case, since the exponents are generated with a built-in ordering, it suffices to consider the $i = 1$ transversal exponent λ_1. The exponents λ_0, λ_1, and λ_i ($i = 2, 3, \ldots 30$) are represented in Fig. 4 as black, red, and gray lines, respectively, as a function of the tunable parameter ϵ. In Fig. 4 we represent only non-negative or vanishing values of the exponents.

Before the loss of transversal stability at $\epsilon_t = 0.192\,50$ all exponents asymptote to nonpositive or vanishing values, indicating that the attractor in the lower energy branch is both periodic (since $\lambda_0 < 0$) and transversely stable (since $\lambda_1 < 0$).

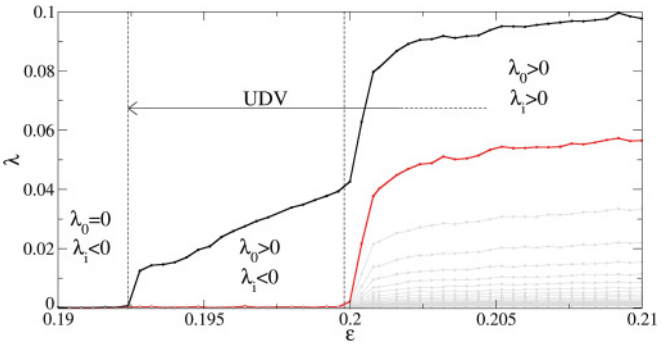

FIG. 4. (Color online) The 30 largest Lyapunov exponents corresponding to modes in Fourier space as a function of ϵ. λ_0, λ_1, and λ_i, $i = 2, 3, \ldots, 30$, are represented as black, red, and gray curves, respectively (from top to bottom).

At the point where the lower energy attractor loses transversal stability λ_0 becomes positive, indicating that the attractor has became temporally chaotic and, at the same time, some periodic orbits embedded in it have lost transversal stability, as will become clearer further on.

Since "most" periodic orbits, however, remain transversely stable, the attractor as a whole is also stable, which is confirmed by $\lambda_1 < 0$ (the fluctuations near the baseline about zero are a numerical artifact). Incidentally, this confirms our claim that the loss of transversal stability of the lower energy attractor occurs through an interior-crisis scenario, since before the transition the attractor is a low-period stable orbit, whereas just after the transition it is a chaotic attractor.

The loss of transversal stability of the lower energy attractor, which happens at $\epsilon_\ell = 0.200\,20$, can be traced out in the Lyapunov diagram of Fig. 4 by the point where λ_1 becomes nonzero, caused by a blowout bifurcation. For $\epsilon > \epsilon_\ell$ "most" transversal exponents become positive, as they should be, since the lower energy attractor stays transversely unstable for all further values of ϵ.

V. UNSTABLE DIMENSION VARIABILITY

Unstable dimension variability in a given chaotic invariant set, like a chaotic attractor, occurs whenever there are embedded periodic orbits with a different number of unstable directions. The relative abundance of periodic orbits with a different number of unstable directions can be evaluated by calculating the corresponding finite-time Lyapunov exponents (FTLE). The FTLEs are computed in the same way as shown in the previous section, but using a finite time span n.

A. A simple example

A characteristic feature of UDV in dynamical systems is the fluctuating behavior (around zero) of the time-n exponent closest to zero. To understand why this is so, let us consider, as a simple example, a two-dimensional map $x \mapsto f(x)$, $y \mapsto g(x,y)$, where $x \in [0,1]$, $y \in \mathbb{R}$, $f(x)$ is a strongly chaotic map (such as the tent, or Bernoulli map), and $g(x,y)$ is a nonlinear function with the symmetry $g(x,-y) = -g(x,y)$. The latter property implies that $y = 0$ is an invariant manifold in which lies the chaotic invariant set (note, however, that, in

what follows, it is not necessary that the manifold be invariant), such that y is the corresponding transversal direction.

The periodic orbits embedded in the chaotic set at $y = 0$ are saddles (with one unstable direction), provided they are transversely stable. On the other hand, let us suppose that some periodic orbit became transversely unstable (as a result of a bifurcation, for example). In this case it will turn into a repeller (two unstable directions), as well as all its infinite pre-images. In this case, the orbit at $y = 0$ is no longer attracting, but it is still a chaotic invariant set due to the skew symmetry of the map. This set displays UDV for it contains an infinite number of both saddles and repellers, densely intertwined.

This occurrence of UDV can be quantitatively assessed through computing the transversal time-n Lyapunov exponent of the map. If we start with an initial condition off but very close to the invariant subspace at $y = 0$, the resulting trajectory visits ϵ-neighborhoods of saddles and repellers of the invariant set for any ϵ, no matter how small, if we iterate the map a large enough number of times. Dividing this long trajectory into nonoverlapping pieces of the same duration n, it turns out that there are time-n segments for which the trajectory is transversely attracting (in average) and others for which it is transversely repelling (also in average).

On computing the time-n Lyapunov exponents along the transversal y direction, the corresponding value of the FTLE along y will be positive (negative) if the trajectory is transversely repelling (attracting) in average. The infinite time limit of the FTLE is the usual transversal Lyapunov exponent. Although the time-n exponent generally takes on a different value, depending on the initial condition we choose, the infinite time limit takes on the same value for almost all initial conditions with respect to the natural ergodic measure of the chaotic invariant set.

The relation between the infinite-time Lyapunov exponent and the FTLEs along the transversal direction y depends on the relative weight of the contribution of both saddles and repellers for the natural measure of the chaotic orbit in the invariant set. Strictly speaking, the onset of UDV occurs when repellers start to appear (after a bifurcation of a former saddle). However, "most" of the periodic orbits (in the measure-theoretical sense) are still saddles. In this situation, the infinite-time Lyapunov exponent along y, which can be regarded as a weighted average of these contributions, is negative. Hence the chaotic set is transversely stable, in spite that some of the orbits (namely, the repellers) are transversely unstable.

As some bifurcation parameter is varied, though, the relative contribution of repellers increases at the same proportion that the contribution of saddles decrease. A quantitative characterization of UDV is provided by the contribution of repellers with respect to that of the saddles. Following this reasoning the UDV is most pronounced when the contributions of saddles and repellers are exactly the same: there will be as many negative as positive values of time-n exponent. Accordingly, the infinite-time exponent along y will be zero at this point, characterizing a blowout bifurcation, and the chaotic set becomes transversely unstable as a whole (this time in spite that some of the orbits—the saddles—are transversely stable).

Varying further the control parameter the contribution of repellers overcomes that of saddles. Though we still have UDV, its intensity is less than in the blowout bifurcation point, and the infinite-time transversal exponent is positive. More values of FTLE along y will be positive than negative. On following this parametric evolution, the end of UDV corresponds to the situation where all periodic orbits in the chaotic set are repellers, such that no time-n exponent will be negative.

B. Drift-wave equation

After describing the parametric evolution of UDV in a simple example, such that the key concepts can be described in the simpler possible way, we now move to the periodically forced and damped drift-wave equation. We have identified two energy branches as distinct manifolds (not necessarily invariant) of the Fourier-mode phase space of the system. The parametric evolution of these manifolds was already described, in the previous two sections, in terms of the loss of transversal stability of these manifolds. Given the concepts related to UDV, however, it is possible to translate that discussion to the framework of UDV, with many conceptual and numerical advantages.

In the same way as we proceeded earlier, we compute, for the temporal low-dimensional chaotic attractor, the FTLE $\tilde{\lambda}_0(n)$ standing for the longitudinal direction (i.e., the direction corresponding to the dynamics in the lower energy state), whereas $\tilde{\lambda}_i(n)$, $(i = 1,2)$, refer to the corresponding transversal exponents. For the sake of notational simplicity we did not indicate explicitly the dependence on the initial condition in the Fourier space, which must, however, always be understood. We focus on both the longitudinal FTLE $\tilde{\lambda}_0(n)$ and the $i = 1$ transversal FTLE $\tilde{\lambda}_1(n)$. Their infinite-time limits are the Lyapunov exponent λ_0 and λ_1, depicted with black and red curves, respectively, in Fig. 4.

Following the same reasoning of the previous example we identify UDV in this system when the time-n Lyapunov exponent in the transversal direction $\tilde{\lambda}_1(n)$ will erratically fluctuate about zero. This suggests the use of a probability density $P(\tilde{\lambda}_1(n))$ for them, so that $P(\tilde{\lambda}_1(n))d\tilde{\lambda}_1$ is the probability that the time-n exponent takes on a value between $\tilde{\lambda}_1$ and $\tilde{\lambda}_1 + d\tilde{\lambda}_1$ for a given n [32].

From this probability distribution we can obtain moments of functions of the time-n exponent, as averages

$$\langle F[\tilde{\lambda}_1(n)]\rangle = \int_{-\infty}^{+\infty} F[\tilde{\lambda}_1(n)]P[\tilde{\lambda}_1(n)]\,d\tilde{\lambda}_1, \qquad (10)$$

assuming proper normalization for $P(\tilde{\lambda}_1(n))$. For n large enough the form of this distribution can be written in the following form:

$$P[\tilde{\lambda}_1(n)] \approx \sqrt{\frac{nG''(\lambda_1)}{2\pi}}e^{-nG[\tilde{\lambda}_1(n)]}, \qquad (11)$$

where the function $G(\lambda_1)$ has the following convexity properties:

$$G(\lambda_1) = G'(\lambda_1) = 0, \quad G''(\lambda_1) > 0. \qquad (12)$$

Expanding G in the vicinity of λ_1, the first nonvanishing term is the quadratic one, and the probability distribution function

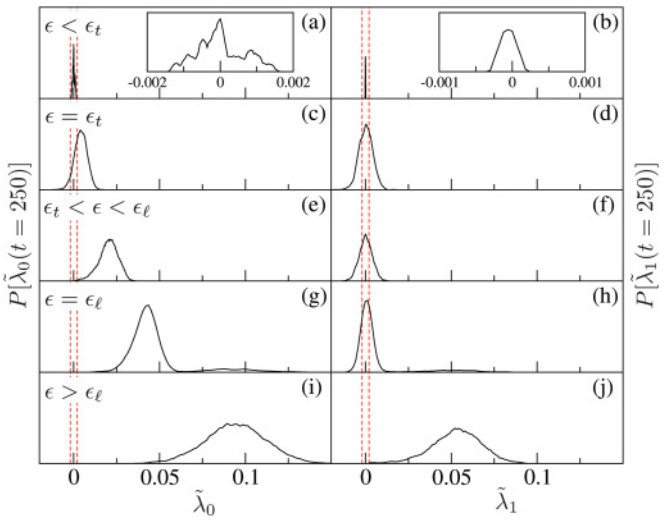

FIG. 5. (Color online) Probability distributions $P(\tilde{\lambda}_i(n))$ for finite-time Lyapunov exponents. Longitudinal exponent $i = 0$: (a) $\epsilon = 0.192$; (c) 0.1925; (e) 0.195; (g) 0.2002; (i) 0.205. Panels (b), (d), (f), (h), and (j) are the corresponding distribution for the $i = 1$ transversal exponent. The dotted red lines indicate the tolerance limits for zero exponents in all cases shown. We depict out of 500 exponent values for each distribution.

has a Gaussian shape

$$P(\tilde{\lambda}_1(n)) \approx \sqrt{\frac{nG''(\lambda_1)}{2\pi}} \exp\left[-\frac{nG''(\lambda_1)}{2}(\tilde{\lambda}_1 - \lambda_1)^2\right], \quad (n \gg 1). \tag{13}$$

Accordingly, the infinite-time limit of the corresponding FTLE is given by $\lambda_1 = \langle\tilde{\lambda}_1(n)\rangle$

We obtained numerical approximations for the probability distribution of both $\tilde{\lambda}_0(n)$ and $\tilde{\lambda}_1(n)$ by considering a large number of trajectories of length n from initial conditions randomly chosen in the chaotic attractor corresponding to the lower energy branch. We actually used a very long trajectory and divide it into small segments to compute the finite-time Lyapunov exponents.

Figures 5(a)–5(j) show some distributions of time-250 exponents of $\tilde{\lambda}_0(n)$ [left panels] and $\tilde{\lambda}_1(n)$ [right panels], obtained for different values of the tunable parameter ϵ. The dashed vertical lines bound the error of the numerical procedure, such that values belonging to the interval within these lines are taken to be zero.

The situation before the onset of UDV is exemplified by Figs. 5(a) and 5(b) since, for this value of $\epsilon = 0.192 < \epsilon_t$, the infinite-time values of both $\tilde{\lambda}_0(n)$ and $\tilde{\lambda}_1(n)$ are nonpositive. As a matter of fact, both distributions are restricted to the interval wherein we consider the exponents equal to zero, as revealed by the magnifications shown as insets in Figs. 5(a) and 5(b). The positive fluctuations shown in these insets are a numerical artifact rather than a dynamical feature, though.

Just after the onset of UDV ($\epsilon = \epsilon_t = 0.19250$) two features appear: (1) the lower energy state becomes chaotic, since the maximum of the distribution function for the longitudinal mode $P[\tilde{\lambda}_0(n)]$ becomes positive [Fig. 5(c)]; (2) the distribution function for the spatial mode $P[\tilde{\lambda}_1(n)]$ starts developing a positive tail [Fig. 5(d)]. The existence of an appreciable number of positive fluctuations of $\tilde{\lambda}_1(n)$ is a fingerprint of UDV in the system. Hence, as soon as the attractor becomes chaotic, it also begins to exhibit UDV.

This is a curious feature of this model in particular since, in most dynamical systems hitherto analyzed the attractor becomes chaotic prior to its becoming hyperchaotic, or exhibiting UDV. The reason for this unusual behavior may be the fact that the chaotic attractor is born, at the point ϵ_t, due to an interior crisis. We have already shown, for a different dynamical system (the kicked double rotor), that UDV can also be created by crises [27].

Figures 5(e) and 5(f) are for the case $\epsilon_t < \epsilon = 0.195 < \epsilon_\ell$ (i.e., long after the onset of UDV), for which the infinite-time values of both $\tilde{\lambda}_0(n)$ and $\tilde{\lambda}_1(n)$ are, respectively, positive and (slightly) negative. The shape of both distributions are Gaussian-like, as expected for n values reasonably large (but not too large so that the distribution reduces to a delta peak, as it should be in the infinite-time limit).

The blowout of the attractor for the lower energy state (at $\epsilon = \epsilon_\ell$) occurs when the maximum of $P[\tilde{\lambda}_1(n)]$ crosses zero [Fig. 5(h)], whereas the other distribution $P[\tilde{\lambda}_0(n)]$ continues to drift toward positive values [Fig. 5(g)]. Even though the former feature cannot be seen directly from Fig. 5(h), it has been found through careful numerical evaluation of the fraction of positive exponents of the corresponding distribution [see Fig. 6(c)].

The blowout bifurcation, as it stands here, is characterized by the fact that just before the blowout bifurcation point the intermittent switchings between the vicinity of the two energy states is a transient phenomenon, followed by an exponential decay to the lower energy state. On the other hand, just after the blowout bifurcation point the intermittent switchings between the vicinity of the two energy states are permanent. It turns out that, at the blowout bifurcation point, half of the finite-time transversal Lyapunov exponents are positive. As a consequence, the lower energy state as a whole loses transversal stability at this point.

Another important feature of the blowout bifurcation is the emergence of a second maximum of the distributions for both $\tilde{\lambda}_0(n)$ and $\tilde{\lambda}_1(n)$ [Figs. 5(g) and 5(h), respectively]. This can be understood by the permanent two-state on-off intermittency existing between the upper and lower energy states. The continuous excursions of the trajectory between such manifolds are reflected in a smaller secondary maximum characterizing the dynamical state in the upper energy state. Finally, after the blowout bifurcation ($\epsilon = 0.205 > \epsilon_\ell$) we have mostly positive fluctuations of both $\tilde{\lambda}_0(n)$ [Fig. 5(i)] and $\tilde{\lambda}_1(n)$ [Fig. 5(j)].

As we have seen in the previous simple example, a quantitative characterization of the UDV may be obtained by computing the relative abundance of saddles and repellers in the chaotic set. This can be accomplished by obtaining the fraction of positive $i = 1$ transversal time-n exponents within a given probability distribution function, or

$$\Phi(n) = \int_0^\infty P[\tilde{\lambda}_1(n)]d\tilde{\lambda}_1(n) \tag{14}$$

shown in Fig. 6(a) as a function of the tunable parameter ϵ as the second uppermost curve. The uppermost curve

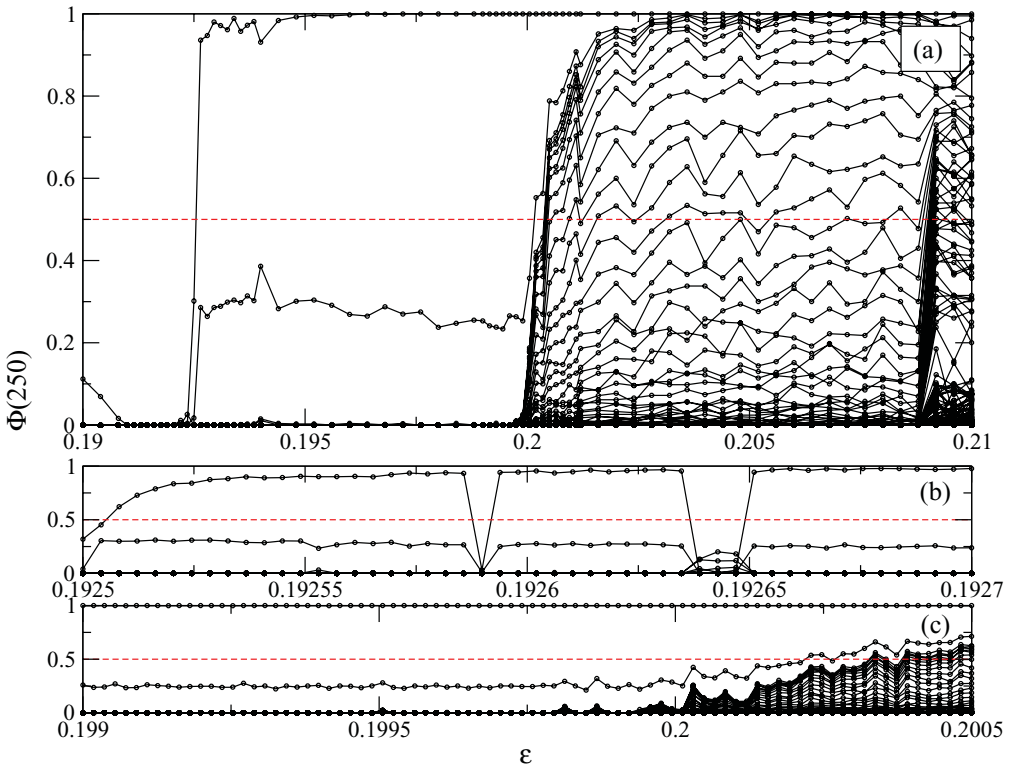

FIG. 6. (Color online) (a) Positive fraction of 30 time-250 Lyapunov exponents as a function of the tunable parameter ϵ. (b) Magnification of the interval surrounding the point marking the onset of UDV in the system. (c) Magnification of the interval surrounding the blowout bifurcation point. The dashed red lines indicate a 50% of positive finite-time exponents.

is the corresponding fraction for the longitudinal exponent $\tilde{\lambda}_0(n)$, and the remaining curves refer to the other transversal Lyapunov exponents, $\tilde{\lambda}_i(n)$, with $i = 2,3,4\ldots$.

For $\epsilon \lesssim \epsilon_t$ this positive fraction of $\tilde{\lambda}_1(n)$ is indeed zero, and the point where it becomes nonzero can be a numerical indicator of the onset of UDV. The sensitivity of this indicator is demonstrated by Fig. 6(b), in which the vicinity of the point ϵ_t is zoomed out. The blowout bifurcation is characterized by this fraction being $1/2$, for exactly half of the time-n exponents are positive at this point. Again, the corresponding value of ϵ_ℓ can be reliably determined from this numerical test [Fig. 6(c)].

VI. CONCLUSIONS

The existence of different energy states (with chaotic dynamics) for a periodically forced and damped drift-wave equation has long been known. It is, in fact, a typical feature of complex systems, since it represents multistable behavior in a high-dimensional phase space, in which two or more chaotic attractors coexist with a generally complicated basin boundary structure. The Fourier-mode phase space offers a convenient geometrical description for this framework since the low-dimensional chaotic attractors can be viewed as belonging to manifolds embedded in the high-dimensional phase space. From this point of view, multistable behavior is affected by the dynamics along the directions transversal to those manifolds.

One observable manifestation of the loss of transversal stability of the multistable chaotic attractors is the existence of intermittent transitions between the coexisting energy states. We have identified this behavior as an instance of the well-known two-state on-off intermittency [10]. The alternations between the vicinities of both energy states have a striking similarity with the previously described hysteretical behavior of trajectories entering this multistable regime. The main difference is that a hysteretical behavior is composed by two transversely *stable* states, while here the behavior is governed by two transversely *unstable* states.

In this work we pushed forward this Fourier phase-space description, by considering the loss of hyperbolicity that occurs in both attractors through a mechanism called unstable dimension variability (UDV). The characteristic feature of UDV is the coexistence of unstable periodic orbits, in a given chaotic set, with different numbers of unstable directions. One of the serious consequences of UDV, whenever it occurs in a given dynamical system, is that computer-generated pseudotrajectories may not (and do not, in fact) shadow true chaotic trajectories of the dynamical system. The loss of shadowability may jeopardize even predictions of a statistical nature.

The occurrence of UDV is thought to be fairly typical in high-dimensional dynamical systems, specially spatiotemporal continuous systems like fluids, plasmas, and waves. The appearance of UDV in the periodically driven and damped drift-wave equation is thus already expected. In this sense, the two-state on-off intermittency becomes an example of chaotic bursting following the occurrence of UDV in a given system.

The intermittent switching between the upper and lower energy states is a nonlinear feature induced by changes of transversal (linear) stability that characterize UDV in the lower energy state. In order to have the two-state on-off intermittency, besides UDV there must be additional nonlinear features, which are the existence of an upper energy state and a chaotic saddle connecting it with the lower energy state undergoing UDV.

We characterized the parametric evolution of UDV through computation of statistical properties of the finite-time Lyapunov exponents in Fourier phase space, which is an important resource when treating high-dimensional systems, for which direct application of bifurcation theory may be utterly impractical. With help of the finite-time Lyapunov exponents we have been able to track three key points in the parametric evolution of UDV, as the driving amplitude is varied (the other parameters being held fixed): its onset, its end, and the point where it is the most intense. At the latter point, also called a blowout bifurcation, the lower energy chaotic state loses transversal stability.

The fact that UDV is the most intense at the blowout point have practical implications, namely, that trajectories are likely to be nonshadowable for an appreciable time interval. Therefore our analysis could find parameter intervals for which the numerical trajectories of the driven and damped drift-wave equation are more or less acceptable, from the shadowing point of view. This is particularly important, inasmuch as most information that can be drawn from such high-dimensional chaotic systems is from numerically generated trajectories.

ACKNOWLEDGMENT

This work was made possible by partial financial support of CNPq, CAPES, Fundação Araucária, and RNF-CNEN (Brazilian Fusion Network).

[1] T. Bohr, M. H. Jensen, G. Paladin, and A. Vulpiani, *Dynamical Systems Approach to Turbulence* (Cambridge University Press, Cambridge, 1998).
[2] U. Frisch, *Turbulence: The Legacy of A. N. Kolmogorov* (Cambridge University Press, Cambridge, 1995).
[3] G. Corso and A. J. Lichtenberg, Phys. Rev. E **59**, 6652 (1999).
[4] S. R. Lopes and F. B. Rizzato, Phys. Rev. E **60**, 5375 (1999).
[5] J. D. Szezech Jr., S. R. Lopes, R. L. Viana, and I. L. Caldas, Physica D **238**, 516 (2009).
[6] M. C. Cross and P. C. Hohenberg, Rev. Mod. Phys. **65**, 851 (1993).
[7] W. Horton, Rev. Mod. Phys. **71**, 735 (1999).
[8] W. Horton and Y. H. Ichikawa, *Chaos and Structures in Nonlinear Plasmas* (World Scientific, Singapore, 1996).
[9] K. He and A. Salat, Plasma Phys. Controlled Fusion **31**, 123 (1989).
[10] P. P. Galuzio, S. R. Lopes, and R. L. Viana, Phys. Rev. Lett. **105**, 055001 (2010).
[11] Y. C. Lai and C. Grebogi, Phys. Rev. E **52**, R3313 (1995).
[12] E. Covas, P. Ashwin, and R. Tavakol, Phys. Rev. E **56**, 6451 (1997).
[13] E. L. Rempel, A. C.-L. Chian, E. E. N. Macau, and R. Rosa, Chaos **14**, 545 (2004).
[14] R. Abraham and S. Smale, Proc. Symp. Pure Math. (AMS) **14**, 5 (1970).
[15] T. Sauer, C. Grebogi, and J. A. Yorke, Phys. Rev. Lett. **79**, 59 (1997).
[16] Y.-C. Lai, C. Grebogi, and J. Kurths, Phys. Rev. E **59**, 2907 (1999).
[17] T. D. Sauer, Phys. Rev. E **65**, 036220 (2002).
[18] R. L. Viana, S. E. de S. Pinto, and C. Grebogi, Phys. Rev. E **66**, 046213 (2002).
[19] S. Dawson, C. Grebogi, T. Sauer, and J. A. Yorke, Phys. Rev. Lett. **73**, 1927 (1994).
[20] W. Horton, Phys. Rep. **192**, 1 (1990).
[21] K. He, Phys. Rev. Lett. **94**, 034101 (2005).
[22] G. Z. dos Santos Lima, Z. O. Guimarães-Filho, I. L. Caldas, I. C. Nascimento, Yu. K. Kuznetsov, A. M. Batista, S. R. Lopes, and R. L. Viana, Phys. Plasmas **19**, 042508 (2009).
[23] K. He and A. C.-L. Chian, Phys. Rev. Lett. **91**, 034102 (2003).
[24] E. L. Rempel and A. C.-L. Chian, Phys. Rev. Lett. **98**, 014101 (2007).
[25] R. L. Viana, C. Grebogi, S. E. de S. Pinto, S. R. Lopes, A. M. Batista, and J. Kurths, Phys. Rev. E **68**, 067204 (2003).
[26] R. F. Pereira, S. E. de S. Pinto, R. L. Viana, S. R. Lopes, and C. Grebogi, Chaos **17**, 023131 (2007).
[27] G. T. Kubo, R. L. Viana, S. R. Lopes, and C. Grebogi, Phys. Lett. A **372**, 5569 (2008).
[28] C. Grebogi, E. Ott, and J. A. Yorke, Physica D **7**, 181 (1983).
[29] R. L. Viana, C. Grebogi, S. E. de S. Pinto, S. R. Lopes, A. M. Batista, and J. Kurths, Physica D **206**, 94 (2005).
[30] G. Benettin, L. Galgani, A. Giorgilli, and J. M. Strelcyn, Meccanica **15**, 21 (1980); I. Shimada and T. Nagashima, Prog. Theor. Phys. **61**, 1605 (1979); A. Wolf, J. B. Swift, H. L. Swinney, and J. A. Vastano, Physica D **16**, 285 (1985).
[31] J. D. Szezech Jr., S. R. Lopes, and R. L. Viana, Phys. Rev. E **75**, 067202 (2007).
[32] E. J. Kostelich, I. Kan, C. Grebogi, E. Ott, and J. A. Yorke, Physica D **109**, 81 (1997).